DENTAL MATERIALS 35 (2019) 893–899

Available online at www.sciencedirect.com

ScienceDirect

journal homepage: www.intl.elsevierhealth.com/journals/dema

Preparation of silica–poly(methyl methacrylate) composite with a nanoscale dual-network structure and hardness comparable to human enamel

*Hiroshi Ikeda**, *Yuki Nagamatsu*, *Hiroshi Shimizu*

Division of Biomaterials, Department of Oral Functions, Kyushu Dental University, Kitakyushu-shi, Fukuoka 803-8580, Japan

ARTICLE INFO

Article history:
Received 18 May 2018
Received in revised form
17 February 2019
Accepted 15 March 2019

Keywords:
Dental restorative material
CAD/CAM
Mesoporous silica
Composite resin
Polymer infiltrated ceramics
Biomimetic

ABSTRACT

Objective. This study aims to prepare an organic–inorganic composite with a nanoscale dual-network structure composed of a ceramic skeleton and infiltrated resin to mimic the mechanical properties of human enamel.

Methods. A porous silica block was obtained by sintering a green body composed of SiO_2 nanoparticles and poly(vinyl alcohol) organic binder. Methyl methacrylate monomers were infiltrated into the porous silica block and thermally polymerized to form poly(methyl methacrylate) (PMMA). A monolithic SiO_2–PMMA composite was obtained, and its nanoscale structure was investigated. Its mechanical properties were characterized by Vickers hardness, elastic modulus, and flexural strength tests.

Results. The SiO_2–PMMA composite had a nanoscale dual-network structure composed of a silica–ceramic skeleton with PMMA-filled continuous 10–20 nm sized pores. The mechanical properties of the composite depended on the SiO_2 content, which could be adjusted by modifying sintering time of the porous silica block. The mechanical properties of the composite exhibited wide variations with Vickers hardness values of 54–756, elastic moduli of 7–54 GPa, and flexural strengths of 75–120 MPa.

Significance. The preparation of a SiO_2–PMMA composite with a dual-network structure at the nanoscale was demonstrated, and the composite was characterized with respect to its hardness compatibility with human enamel.

1. Introduction

Organic–inorganic composite materials for dental restorations have been extensively studied over the past decades [1,2]. With recent advances in computer-aided design/computer-aided manufacturing (CAD/CAM) systems, many CAD/CAM composites with superior mechanical properties have been developed for indirect restorative materials such as dental crowns [3–5]. The CAD/CAM composites used for crown restorations are required to exhibit mechanical properties similar to those of human enamel for a successful biomimetic restoration. To mimic the mechanical properties of human enamel, both hardness and elastic modulus are important factors. These mechanical properties of composite materials depend on the

* *Corresponding author.*
E-mail address: r16ikeda@fa.kyu-dent.ac.jp (H. Ikeda).

https://doi.org/10.1016/j.dental.2019.03.006

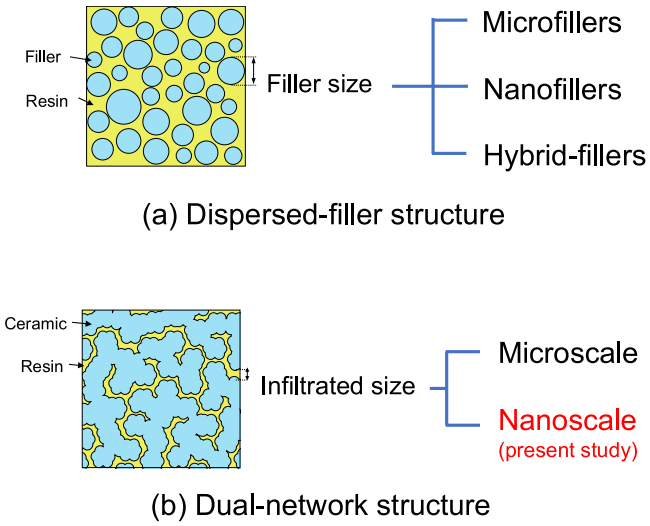

Fig. 1 – Classification of dental organic–inorganic composites: (a) dispersed-filler (DF) structure and (b) dual-network (DN) structure.

complexes and microstructures of the organic and inorganic components. The composite structure of dental CAD/CAM composites can be roughly classified into two groups [4]: dispersed-filler (DF) and dual-network (DN) structure, which are drawn schematically in Fig. 1.

The DF structure shown in Fig. 1(a) is composed of a polymer matrix with dispersed inorganic fillers. This DF structural category can be further sub-divided into four or more groups based on the filler size: nanofiller (<100 nm), microfiller (>several μm), hybrid fillers containing both nanofillers and microfillers, and nanocluster fillers made from a mixture of nanofiller and polymer. Many practical and commercial products have been developed using DF composites, although differences exist in filler size, composition, content, and polymer matrix [2]. Meanwhile, the DF structure of the composites is mechanically compatible with human dentin and not with human enamel [3,6].

The DN structure is shown in Fig. 1(b) and is composed of co-continuous phases of ceramic skeleton and resins. DN structure is generally fabricated by infiltrating monomers into the continuous pores of pre-sintered ceramics, followed by polymerization [7]. Due to this unique fabrication process, the DN structure formed in the composites is called a polymer infiltrated ceramic network (PICN) [8]. The mechanical properties of the DN structural composites are closer to those of enamel, compared with those of the DF structure. Indeed, many basic investigations demonstrated that the PICN structures of Vita Enamic and related materials exhibit similar mechanical properties to those of human enamel [9–15]. These results suggest that the DN (or PICN) structural composite would be suitable for mimicking human enamel, at least in terms of its mechanical properties. Although DN structures can be further sub-divided based on the complex scale of the ceramics and polymers, they are limited in terms of structural types to the micrometer scale. Therefore, no reports on the enamel bio-mimic mechanical properties of DN composite materials at the nanoscale have been published.

This study aims to prepare a novel organic–inorganic composite with DN structure at the nanoscale (Fig. 1) to mimic the mechanical properties of human enamel. To achieve the ideal goal, a novel preparation process was first developed, as described in Fig. 2. Silica (SiO_2) and poly(methyl methacrylate) (PMMA) were chosen as the inorganic and organic compo-

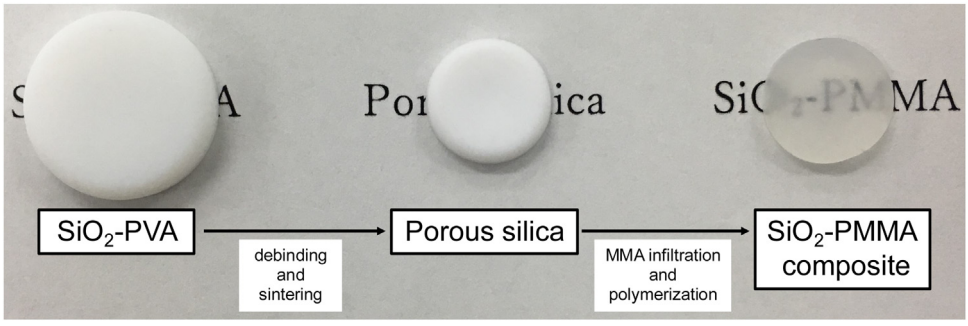

Fig. 2 – Flow chart of the preparation process of the SiO_2–PMMA composite via porous silica and PMMA infiltration.

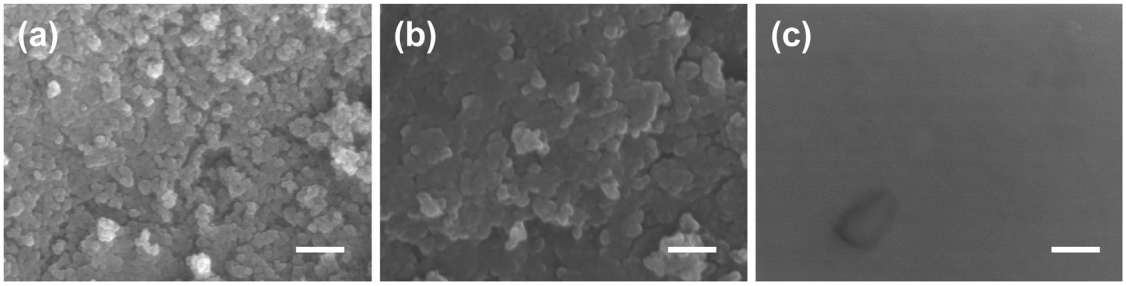

Fig. 3 – FE-SEM images of the porous silica blocks obtained by sintering the SiO_2–PVA green body at 1130 °C for (a) 1 min, (b) 4 h, and (c) 5 h. The scale bar indicates 300 nm.

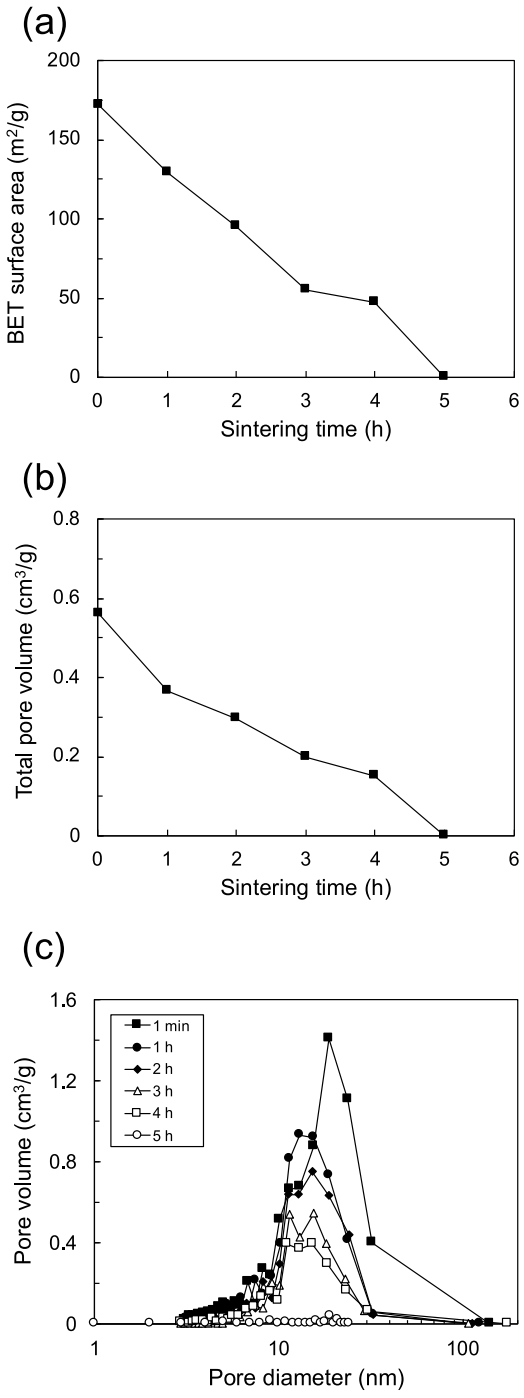

Fig. 4 – (a) BET surface area, (b) total pore volume, and (c) pore size distributions of the porous silica blocks obtained by nitrogen sorption measurements via the BJH method using a porosimeter. The porous silica blocks were fabricated by thermal debinding the SiO_2–PVA green body at 600 °C followed by sintering at 1130 °C for a given time.

nents of the composite, respectively. To demonstrate the bio-mimicking mechanical properties of the novel SiO_2–PMMA composite, we evaluated the hardness and elastic modulus of the prepared composite and addressed the possibility for mimicking human enamel.

2. Material and methods

2.1. *Preparation of the SiO_2–PMMA composite*

Fig. 2 shows a simple overview of the preparation procedure of the SiO_2–PMMA composite. First, the SiO_2–poly(vinyl alcohol) (PVA) green body was prepared, then debinded and sintered to form a porous silica block. Subsequently, liquid methyl methacrylate (MMA) was infiltrated into the porous silica block, followed by thermal polymerization, to obtain the SiO_2–PMMA composite.

Six grams of fumed silica nanoparticles with a mean diameter of 7 nm (Aerosil 300, Nippon Aerosil, Japan) was added to 54 g of purified water at pH 3 and dispersed under ultrasonication for 1 h. Meanwhile, 11.4 g of a 10 wt% PVA solution was obtained by dissolving a PVA powder (Wako Pure Chemical, Japan) in purified water. The prepared SiO_2 suspension and PVA solution were mixed using a magnetic stirrer at 30 °C for 24 h, resulting in a SiO_2–PVA slurry. The slurry was then poured into a Teflon container and dried in an oven at 30 °C for 7 days. Consequently, a solid-state monolithic SiO_2–PVA green body was obtained.

Thermal debinding of the fabricated SiO_2–PVA green body was performed in an electric furnace at 600 °C for 3 h in air; this process combusts the PVA binder in the green body. By following this debinding process, the green body was sintered to form a porous silica block at 1130 °C in air for a given time (1 min, 1 h, 2 h, 3 h, 4 h, or 5 h). The detailed fabrication process for the SiO_2–PVA green body and silica blocks is described in previous reports [16,17].

The resulting porous silica block was immersed in MMA (Wako Pure Chemical, Japan) dissolved with 0.5 wt% benzoyl peroxide (BPO, Alfa Aesar, USA) at room temperature. The infiltration behavior of the MMA into the porous silica block was monitored by the naked eye because the appearance of the block was changed from opaque to transparent following MMA impregnation. After immersion for 24 h, the MMA infiltrated block looked transparent. Prior to thermal polymerization, the MMA infiltrated block was removed from the BPO-containing MMA solution and immersed in another MMA solution without BPO. Thermal polymerization of the MMA infiltrated block was performed at 60 °C while immersed in the MMA solution. In this "inside-out polymerization process," the MMA infiltrated into the silica was polymerized gradually from the inside to the outside because the BPO concentration in the MMA decreased from the inside to the outside of the composite. This BPO concentration gradient resulted from the immersion of the MMA-infiltrated silica in BPO-free MMA solution. During polymerization, the surrounding MMA gradually infiltrated the composite in accordance with polymerization shrinkage. As a result, pore generation owing to polymerization shrinkage could be moderated and a dense composite was obtained. After adequate polymerization time, excess PMMA on the sample surface was removed by mechanically polishing or cutting. Note that no silane treatment was performed to prepare the composite. Finally, the transparent SiO_2–PMMA composite block was obtained, as shown in Fig. 2.

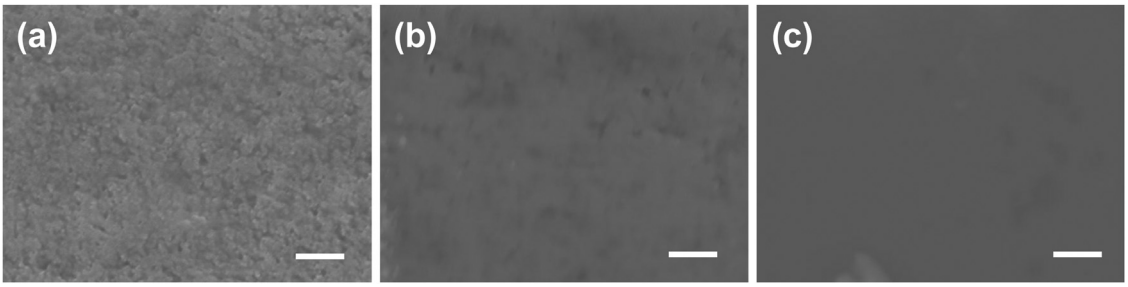

Fig. 5 – FE-SEM images of the SiO_2–PMMA composites obtained from the porous silica blocks sintered at 1130 °C for (a) 1 min, (b) 4 h, and (c) 5 h. The scale bar indicates 300 nm.

2.2. *Characterization of the SiO_2–PMMA composite*

To identify the complex structure of the prepared samples, both the silica block and SiO_2–PMMA composite were evaluated as follows. The morphologies of the silica block and SiO_2–PMMA composite were observed by field emission scanning electron microscopy (FE-SEM, JSM-6340F, JEOL, Japan). The surface area and pore size distribution of the samples were calculated using the Brunauer–Emmett–Teller (BET) method [18] and the Barrett–Joyner–Halenda (BJH) method [19], respectively, using nitrogen adsorption–desorption isotherms obtained using a nitrogen sorption porosimeter (QuadraSorb SI, Quantachrome Instruments, USA). The total pore volume of the samples was also obtained from the isotherms.

The degree of conversion (DC) of C=C bonds in PMMA of the SiO_2–PMMA composite was determined using a Fourier transform infrared (FT-IR) spectrometer (FT/IR-6300, Jasco, Japan) with a diffuse reflectance apparatus. Two characteristic bands 1637 cm^{-1} (stretching of methyl methacrylate C=C) and 1720 cm^{-1} (stretching of carbonyl group C=O) were used to calculate the DC of polymerization [20]. The ratios of absorbance intensities were calculated before and after polymerization using the following equation:

$$DC\,(\%) = \left(1 - \frac{[A(C=C)/A(C=O)]_{polymer}}{[A(C=C)/A(C=O)]_{monomer}}\right) \times 100$$

where A(C=C) is the absorbance intensity of the methyl methacrylate peak and A(C=O) is the absorbance intensity of the internal standard peak. All measurements were performed eight times.

The elastic modulus and flexural strength of the prepared samples were determined by a three-point bending test according to ISO 10477: 2004. Each SiO_2–PMMA composite was cut into a bar shape 25 × 2 × 2 mm in size using a diamond wheel saw and polished using emery papers. The bar specimens (n = 8) were loaded until fracture using a mechanical testing device (AGS-H, Shimadzu Corp., Tokyo, Japan) at crosshead speed of 1 mm/min with a three-point bending setup (20-mm supporting span). The fractured specimens after the flexural strength measurements were subjected to a Vickers hardness measurement. The Vickers hardness (Hv) of the SiO_2–PMMA composite was examined using a hardness tester (HMV-G21ST, Shimadzu, Japan) with an applied load of 1.96 N for 15 s. The measurements were performed in triplicated on each specimen (total n = 24 for obtaining each value).

The amount of inorganic filler in the SiO_2–PMMA composite was determined by a calcination method as follows. Each hardness-tested-specimen was weighed using an electric balance. Subsequently, the specimens were heat-treated at 700 °C for 5 h in air to burn the organic matter (PMMA). After the heat-treatment, the weight of residue was measured and the inorganic content was calculated from the difference between the specimen weights before and after heat-treatment (n = 8). In this study, it was assumed that the obtained inorganic content was equal to that of SiO_2.

2.3. *Statistical analysis*

The results were analyzed by one-way analysis of variance (ANOVA) followed by Tukey multiple comparison test, using statistical software EZR (Saitama Medical Center, Japan) [21]. The significance level was set at 0.05 for all analyses.

Weibull analysis was carried out for the results of flexural strength by using statistical software Minitab 18 (Minitab Inc, USA). The Weibull distribution is given by following equation

$$\ln\ln\frac{1}{1-P_n} = m\ln\sigma - m\ln\sigma_0$$

$$P_n = \frac{n-0.5}{N}$$

where σ is the flexural strength, m is Weibull modulus, σ_0 is the characteristic strength, P_n is the failure probability, n is the ranking, and N is the total number of test samples.

3. Results

3.1. *Nanostructure of the SiO_2–PMMA composite*

The nanostructure of the porous silica blocks was examined using FE-SEM and the results are shown in Fig. 3. For the sample shown in Fig. 3(a), it was confirmed that the silica nanoparticles were linked to each other and formed a silica-skeleton network several tens of nanometers in size. In addition, interspaces within the silica skeleton network can be seen. In Fig. 3(b) for the sample obtained after sintering for 4 h, a porous structure was also observed. Compared to the porous structures shown in Fig. 3(a) and (b), the silica skeleton size for

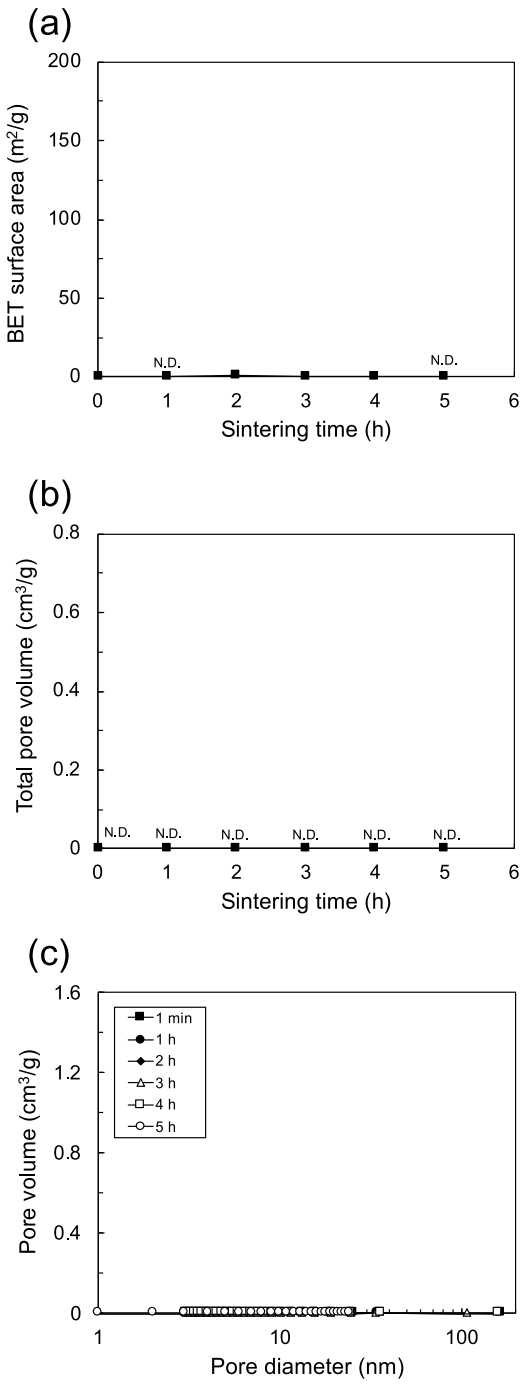

Fig. 6 – (a) BET surface area, (b) total pore volume, and (c) pore size distributions of the SiO_2–PMMA composites obtained by nitrogen sorption measurements via the BJH method using a porosimeter. The SiO_2–PMMA composites were fabricated using the porous silica blocks sintered at 1130 °C for (a) 1 min, (b) 4 h, and (c) 5 h.

the 4 h sintered silica (Fig. 3(a)) is larger than that of the 1 min sintered silica (Fig. 3(b)). On the other hand, for the silica block obtained by sintering for 5 h, interspaces between the silica skeleton were diminished and a denser structure was formed.

The interspaces within the silica-skeleton network of the silica blocks were further examined by nitrogen adsorption–desorption isotherm measurements and the results are shown in Fig. 4(a)–(c) for the BET surface areas, total pore volume, and pore size distribution, respectively. The BET surface area (Fig. 4(a)) and total pore volume (Fig. 4(b)) of the silica blocks decreased with increasing sintering time. Fig. 4(c) shows that the pores sizes for all samples are distributed from approximately 10–20 nm, with no pore larger than 40 nm. The intensities of the distribution peak of the silica blocks decrease with increasing sintering time. These results indicate that the silica blocks exhibit opened and continuous nanosized pores, and their porosity is changed by sintering time.

Fig. 5 shows the FE-SEM images of the SiO_2–PMMA composite prepared by MMA infiltration into the porous silica block followed by thermal polymerization. In contrast to the structure of the silica blocks, the SiO_2–PMMA composite, as shown in Fig. 5(a) and (b), formed a dense structure without apparent pores; although a mixture of silica skeleton and infiltrated PMMA structures was observed. Meanwhile, Fig. 5(c) shows that a glassy structure was observed in the prepared sample.

Fig. 6 shows the BET surface areas, total pore volume, and pore size distribution of the SiO_2–PMMA composites. As shown in Fig. 6(a) and (b), the values of the BET surface area and total pore volume are almost zero for all examined SiO_2–PMMA composites. In addition, the pore size distributions shown in Fig. 6(c) indicate that no pores were detected over the examined range.

The SiO_2 content of the SiO_2–PMMA composite as a function of sintering time determined by the combustion method is given at Table 1. The SiO_2 content increased with increasing sintering time from 46 to 100 wt%.

The results for DC of PMMA of SiO_2–PMMA composites are listed in Table 1. The DC values were independent of the sintering time and SiO_2 content. The DC values of the composites were ca. 73–77, which are lower than those of PMMA-based resins prepared by thermal polymerization (ca. 90–97%) [22,23], but higher than those of light-cured resins (ca. 50–70%) [20,24,25].

3.2. *Mechanical properties of the SiO_2–PMMA composite*

The results of multiple comparisons of the mechanical properties of each composite are shown in Table 1. The Vickers hardness and flexural strength tend to increase with SiO_2 content. The Vickers hardness value of the composite was sensitive to the SiO_2 content and increased with increasing SiO_2, ranging from 54 to 756. The elastic modulus also increased with increasing SiO_2 content from 7 to 54 GPa and the strength increased slightly with SiO_2 content in the range of 75–120 MPa. Table 2 shows the results of Weibull analysis of the flexural strength of composites. A high Weibull modulus suggests the homogeneity of the blocks. The Weibull modulus values of the SiO_2–PMMA composites are ca. 6–12. These values are close to those of other polymer-infiltrated ceramics (m = 5–12) [7].

4. Discussion

The complex structure of the SiO_2–PMMA composite can be explained as follows, based on the evaluation of the porous

Table 1 – Mean values (standard deviation) of degree of conversion, SiO_2 content, and mechanical properties for the SiO_2–PMMA composites.

Sintering conditions for porous silica	SiO_2 content (wt%)	Degree of conversion (%)	Vickers hardness (–)	Elastic modulus (GPa)	Flexural strength (MPa)
1130 °C, 1 min	46.0 (0.5) a	76.8 (1.9)	54.2 (2.8) a	6.9 (0.8) a	74.4 (9.3) a
1130 °C, 1 h	71.4 (1.2) b	75.1 (2.5)	157.3 (8.2) b	20.5 (0.9) b	84.6 (10.2) ab
1130 °C, 2 h	82.7 (2.1) c	72.8 (3.2)	243.6 (48.9) c	26.4 (3.7) c	85.3 (12.2) ab
1130 °C, 3h	83.9 (2.7) c	74.5 (3.3)	317.7 (53.6) d	26.2 (2.8) c	93.3 (12.9) b
1130 °C, 4 h	85.8 (1.9) c	73.0 (3.3)	396.5 (76.7) e	27.8 (3.2) c	92.3 (8.4) b
1130 °C, 5 h	100 (0.2) d	–	756.8 (73.0) f	53.5 (3.0) d	119.2 (10.2) c

Different letters represent a significant difference between the groups ($p < 0.05$). n = 8 for degree of conversion, SiO_2 content, elastic modulus and flexural strength. n = 24 for Vickers hardness.

Table 2 – Weibull analysis of the flexural strength of the SiO_2–PMMA composites.

Sintering conditions for porous silica	Weibull modulus, m (–)	95% CI of m (–)	Characteristic strength, S_0 (MPa)	95% CI of S_0 (MPa)
1130 °C, 1 min	8.6	5.0–14.5	78.6 a	72.2–85.7
1130 °C, 1 h	9.6	5.7–16.2	89.0 a	82.4–96.1
1130 °C, 2 h	6.5	4.0–10.6	90.9 ab	81.2–101.7
1130 °C, 3 h	8.5	4.9–14.6	98.9 b	90.7–107.9
1130 °C, 4 h	12.0	7.1–20.3	96.1 b	90.4–102.1
1130 °C, 5 h	11.7	7.1–19.3	124.0 c	116.4–132.1

Different letters represent a significant difference between the groups.
CI; confidence interval.

silica blocks and SiO_2–PMMA composites. Figs. 3 and 4 show that the silica blocks exhibited the porous structure with silica skeleton networks on the order of tens of nanometers. Considering the SiO_2 nanoparticles used as a starting material were 7 nm in size, the skeleton network of porous silica is likely composed of consolidated sintered nanoparticles. Comparing the silica skeleton sizes between samples in Fig. 3(a) and (b), the silica skeleton grew larger with increasing sintering time. In contrast to the porous structure of the silica block, the SiO_2–PMMA composite exhibited a dense structure without nanosized pores, as shown in Figs. 5 and 6. This suggests that the PMMA filled in the continuous nanosized pores. This can also be judged from the appearance of the prepared SiO_2–PMMA composite. As indicated in the photograph of the SiO_2–PMMA composite shown in Fig. 2, the SiO_2–PMMA composite was transparent, while the porous silica block was opaque. Generally, the optical transparency of an organic–inorganic composite is affected by the difference in refractive indices between the organic and inorganic components. For the porous silica block, the difference of the refractive indices between silica (n = 1.46) and air (n = 1) is relatively high. This mismatch leads to light scattering at the interface, making the silica block appear opaque. For the SiO_2–PMMA composite, the difference in the refractive indices between the silica (n = 1.46) and PMMA (n = 1.49) is relatively low, resulting in low light scattering at the interface if the PMMA fills the pores of the silica block. Therefore, the SiO_2–PMMA composite was optically transparent which indicates that it possessed nanosized structure composed of an infiltrated PMMA network and silica skeleton network with sintered nanoparticles. Thus, the structure of the SiO_2–PMMA composite should be classified as having DN structure (PICN structure) at the nanoscale, as shown in Fig. 1.

Table 3 – Vickers hardness and elastic modulus of the prepared SiO_2–PMMA composite, human enamel [26], and human dentin [26].

	Vickers hardness (–)	Elastic modulus (GPa)
SiO_2–PMMA	54–756	7–54
Human enamel	ca. 300–500	ca. 40–100
Human dentin	ca. 50–100	ca. 10–30

The mechanical properties (Vickers hardness, elastic modulus, and flexural strength) of the SiO_2–PMMA composite were dependent on the SiO_2 content, as shown in Table 1. The SiO_2 content in the SiO_2–PMMA composite can be controlled by adjusting the sintering time of the porous silica block. Meanwhile, there are no differences between the DC values of the composite, as listed in Table 1. Thus, the mechanical properties of the SiO_2–PMMA composite can be controlled by changing the sintering time of the porous silica block and the SiO_2 content.

The prepared SiO_2–PMMA composite with DN structure at the nanoscale can provide mechanical compatibility with human enamel and dentin. As listed in Table 3, the Vickers hardness and elastic modulus of the fabricated SiO_2–PMMA composite were compared to those of human enamel. The mechanical properties of real human enamel vary over a wide range [26]. Similarly, the mechanical properties of the SiO_2–PMMA composite can be significantly varied by changing the SiO_2 content, as mentioned above. For instance, the SiO_2–PMMA composite with 46 wt% SiO_2 exhibited a Vickers

hardness of 54 and elastic modulus of 7 GPa, which correspond to the values of human dentin. At 86 wt% SiO_2, the Vickers hardness and elastic modulus are 397 and 28 GPa, respectively. This Vickers hardness value is comparable to that of human enamel, while the elastic modulus value is slightly less than that of enamel. Thus, this SiO_2–PMMA composite was compatible with enamel in terms of hardness and with hard dentin with respect to elastic modulus. The sample composed of almost 100 wt% SiO_2 showed a Vickers hardness of 757, higher than that of enamel, and an elastic modulus of 54 GPa, which is comparable to that of enamel.

In summary, it was demonstrated that the SiO_2–PMMA composite with a dual-network structure at the nanoscale exhibited mechanical compatibility with human enamel in terms of the hardness. However, its elastic modulus was slightly less than that of human enamel. In future studies, the elastic modulus of the composite should be able to reach to that of human enamel by substituting silica with high-modulus ceramics such as alumina or zirconia. The organic–inorganic composite with the nanoscale dual-network structure has potential applications for mimicking human enamel and dentin.

5. Conclusions

The novel SiO_2–PMMA composite with a dual-network structure at the nanoscale was successfully prepared via MMA infiltration into a pre-sintered porous silica block followed by thermal polymerization to form PMMA. The mechanical properties of the composite were affected by the SiO_2 content, which can be controlled by changing the sintering time of the porous silica block. By optimizing the preparation conditions, the SiO_2–PMMA composite achieved compatible hardness with that of human enamel and an elastic modulus similar to that of human dentin.

Acknowledgments

This work was supported in part by the Japanese Association for Dental Science. The author (H. Ikeda) is thankful for the Basic Science Research Projects from the Sumitomo Foundation (Grant No. 160908).

REFERENCES

[1] Chen MH. Update on dental nanocomposites. J Dent Res 2010;89:549–60.
[2] Ferracane JL. Resin composite — state of the art. Dent Mater 2011;27:29–38.
[3] Ruse ND, Sadoun MJ. Resin-composite blocks for dental CAD/CAM applications. J Dent Res 2014;93:1232–4.
[4] Mainjot AK, Dupont NM, Oudkerk JC, Dewael TY, Sadoun MJ. From artisanal to CAD-CAM blocks: state of the art of indirect composites. J Dent Res 2016;95:487–95.
[5] Miyazaki T, Hotta Y, Kunii J, Kuriyama S, Tamaki Y. A review of dental CAD/CAM: current status and future perspectives from 20 years of experience. Dent Mater J 2009;28:44–56.
[6] Lauvahutanon S, Takahashi H, Shiozawa M, Iwasaki N, Asakawa Y, Oki M, et al. Mechanical properties of composite resin blocks for CAD/CAM. Dent Mater J 2014;33:705–10.
[7] Nguyen JF, Ruse D, Phan AC, Sadoun MJ. High-temperature-pressure polymerized resin-infiltrated ceramic networks. J Dent Res 2014;93:62–7.
[8] El Zhawi H, Kaizer MR, Chughtai A, Moraes RR, Zhang Y. Polymer infiltrated ceramic network structures for resistance to fatigue fracture and wear. Dent Mater 2016;32:1352–61.
[9] He LH, Swain M. A novel polymer infiltrated ceramic dental material. Dent Mater 2011;27:527–34.
[10] He LH, Purton D, Swain M. A novel polymer infiltrated ceramic for dental simulation. J Mater Sci — Mater Med 2011;22:1639–43.
[11] Coldea A, Swain MV, Thiel N. Mechanical properties of polymer-infiltrated-ceramic-network materials. Dent Mater 2013;29:419–26.
[12] Dirxen C, Blunck U, Preissner S. Clinical performance of a new biomimetic double network material. Open Dent J 2013;7:118–22.
[13] Della Bona A, Corazza PH, Zhang Y. Characterization of a polymer-infiltrated ceramic-network material. Dent Mater 2014;30:564–9.
[14] Albero A, Pascual A, Camps I, Grau-Benitez M. Comparative characterization of a novel cad-cam polymer-infiltrated-ceramic-network. J Clin Exp Dent 2015;7:e495–500.
[15] Lawson NC, Bansal R, Burgess JO. Wear, strength, modulus and hardness of CAD/CAM restorative materials. Dent Mater 2016;32:e275–83.
[16] Ikeda H, Fujino S, Kajiwara T. Preparation of SiO_2-PVA nanocomposite and monolithic transparent silica glass by sintering. J Ceram Soc Jpn 2011;119:65–9.
[17] Ikeda H, Fujino S. Composition and pH dependence on aggregation of SiO_2-PVA suspension for the synthesis of porous SiO_2-PVA nanocomposite. J Porous Mater 2014;21:1143–9.
[18] Brunauer S, Emmett PH, Teller E. Adsorption of gases in multimolecular layers. J Am Chem Soc 1938;60:309–19.
[19] Barrett EP, Joyner LG, Halenda PP. The determination of pore volume and area distributions in porous substances. 1. Computations from nitrogen isotherms. J Am Chem Soc 1951;73:373–80.
[20] Viljanen EK, Skrifvars M, Vallittu PK. Degree of conversion of a copolymer of an experimental monomer and methyl methacrylate for dental applications. J Appl Polym Sci 2004;93:1908–12.
[21] Kanda Y. Investigation of the freely available easy-to-use software 'EZR' for medical statistics. Bone Marrow Transplant 2012;48:452–8.
[22] Bartoloni JA, Murchison DF, Wofford DT, Sarkar NK. Degree of conversion in denture base materials for varied polymerization techniques. J Oral Rehabil 2000;27:488–93.
[23] Leao RS, de Moraes SLD, Aquino K, Isolan CP, Casado B, Montes M. Effect of pressure, post-pressing time, and polymerization cycle on the degree of conversion of thermoactivated acrylic resin. Int J Dent 2018;2018:5743840.
[24] Yoon T, Lee Y, Lim B, Kim C. Degree of polymerization of resin composites by different light sources. J Oral Rehabil 2002;29:1165–73.
[25] Ribeiro B, Boaventura J, Brito-Gonçalves J, Rastelli A, Bagnato V, Saad J. Degree of conversion of nanofuilled and microhybrid composite resins photo-activated by different generations of LEDs. J Appl Oral Sci 2012;20:212–7.
[26] Zhang Y-R, Du W, Zhou X-D, Yu H-Y. Review of research on the mechanical properties of the human tooth. Int J Oral Sci 2014;6:61–9.